Journal of Molecular Graphics and Modelling 30 (2011) 15–23

Contents lists available at ScienceDirect

Journal of Molecular Graphics and Modelling

journal homepage: www.elsevier.com/locate/JMGM

The effect of β-saturated pyrrolic rings on the electronic structures and aromaticity of magnesium porphyrin derivatives: A density functional study

Liang Wan, Dongdong Qi, Yuexing Zhang*

Department of Chemistry, University of Science and Technology Beijing, Beijing 100083, China

ARTICLE INFO

Article history:
Received 10 March 2011
Received in revised form 24 May 2011
Accepted 27 May 2011
Available online 12 June 2011

Keywords:
Magnesium porphyrin
Density functional theory
β-Saturated pyrrolic rings
Electronic structure
Aromaticity

ABSTRACT

Density functional theory (DFT) calculation on the molecular structures, molecular orbitals, electronic absorption spectra, and magnetic properties of magnesium porphyrin (MgPor) and a series of five hydrogenated magnesium porphyrin complexes with different number of β-saturated pyrrolic rings, namely MgPor-β-1Hy, MgPor-β-opp-2Hy, MgPor-β-adj-2Hy, MgPor-β-3Hy, and MgPor-β-4Hy, clarifies the red-shift of the lowest energy absorption band from chlorophyll *a* to bacteriochlorophyll and reveals the strong chemical stability for both of them. The energy levels of highest occupied molecular orbitals (HOMO) and HOMO−1 for MgPor are reversed upon hydrogenation at β-positions (2 and 3, 7 and 8, 12 and 13, and 17 and 18) of porphyrin ring. Along with the increase of β-saturated pyrrolic rings from 1, 2, 3, to 4, the HOMO energy increases from −4.78 eV to −3.10 eV in a regular manner. In contrast, the lowest unoccupied molecular orbitals (LUMO) energy levels of MgPor, MgPor-β-1Hy, and MgPor-β-opp-2Hy are very similar with each other. As a result, the lowest energy absorption band involving main transition from HOMO to LUMO is red-shifted from MgPor-β-1Hy to MgPor-β-opp-2Hy which is representative of chlorophyll *a* and bacteriochlorophyll, respectively. Natural hydroporphyrins represented by MgPor, MgPor-β-1Hy, and MgPor-β-opp-2Hy have turned out to be aromatic and stable enough, in good accordance with the ubiquity of their derivatives in the nature. In contrast, MgPor-β-adj-2Hy, MgPor-β-3Hy, and MgPor-β-4Hy with relatively weak aromaticity seem to be unstable and therefore were not found in nature.

1. Introduction

Natural metalloporphyrin derivatives have been at the focus of multidisciplinary interest over the last one century due to their diverse functions in biological processes [1–6]. In particular, the two porphyrinato magnesium complexes, chlorophyll *a* and bacteriochlorophyll, play important roles in plant and bacterial photosynthesis, respectively [4–6].

Chlorophyll *a* has strong lowest energy absorption band at ca. 660 nm, while this band is significantly red-shifted to 772 nm in the electronic absorption spectrum of bacteriochlorophyll [7,8]. The primary structural difference between the two molecules is that bacteriochlorophyll has two β-saturated pyrrolic rings at the opposite positions, while chlorophyll *a* has only one (Fig. S1, supplementary data). It seems that hydrogenation of two opposite pyrrole rings could lead to the red-shift of the "orange" peak of chlorophyll *a*. In 2000, Jusélius and Sundholm studied the aromatic pathways of magnesium porphyrin, magnesium chlorin, and magnesium bacteriochlorins by performing aromatic ring current shieldings (ARCS) and nucleus independent chemical shift (NICS) calculations [9]. However, many problems still remain unresolved such as the contradiction of the large current susceptibility with the high-lying energy for Mg4BC (MgPor-β-4Hy) as compared to other magnesium porphyrins. In 2001, Parusel and Grimme concluded that the experimentally observed large intensity of the Q-band for the hydroporphyrins is due to a relaxation of the near-degeneracy of the four frontier molecular orbitals based on their DFT/MRCI calculations [10]. In 2004, Linnanto and Korppi-Tommola found that the Zindo/S CIS method for the structures of chlorophylls and bacteriochlorophylls optimized by PM5 method is a computationally efficient approach to produce acceptable electronic transition energies as compared to experimental results [11]. In 2006, Petit et al. undertook a systematic study on the excited states of metal free porphyrin, metal free chlorine, and metal free bacteriochlorin using the time dependent density functional theory (TDDFT) method [12]. Up to now, there seems still no report on the theoretical investigation towards understanding the relationship between hydrogenation and electronic absorption spectra as well as hydrogenation and aromaticity of derivatives, to the best of our knowledge.

* Corresponding author. Tel.: +86 10 6233 2681; fax: +86 10 6233 2462.
E-mail addresses: yxzhang@ustb.edu.cn, zhangyuexing@sdu.edu.cn (Y. Zhang).

1093-3263/$ – see front matter © 2011 Elsevier Inc. All rights reserved.
doi:10.1016/j.jmgm.2011.05.003

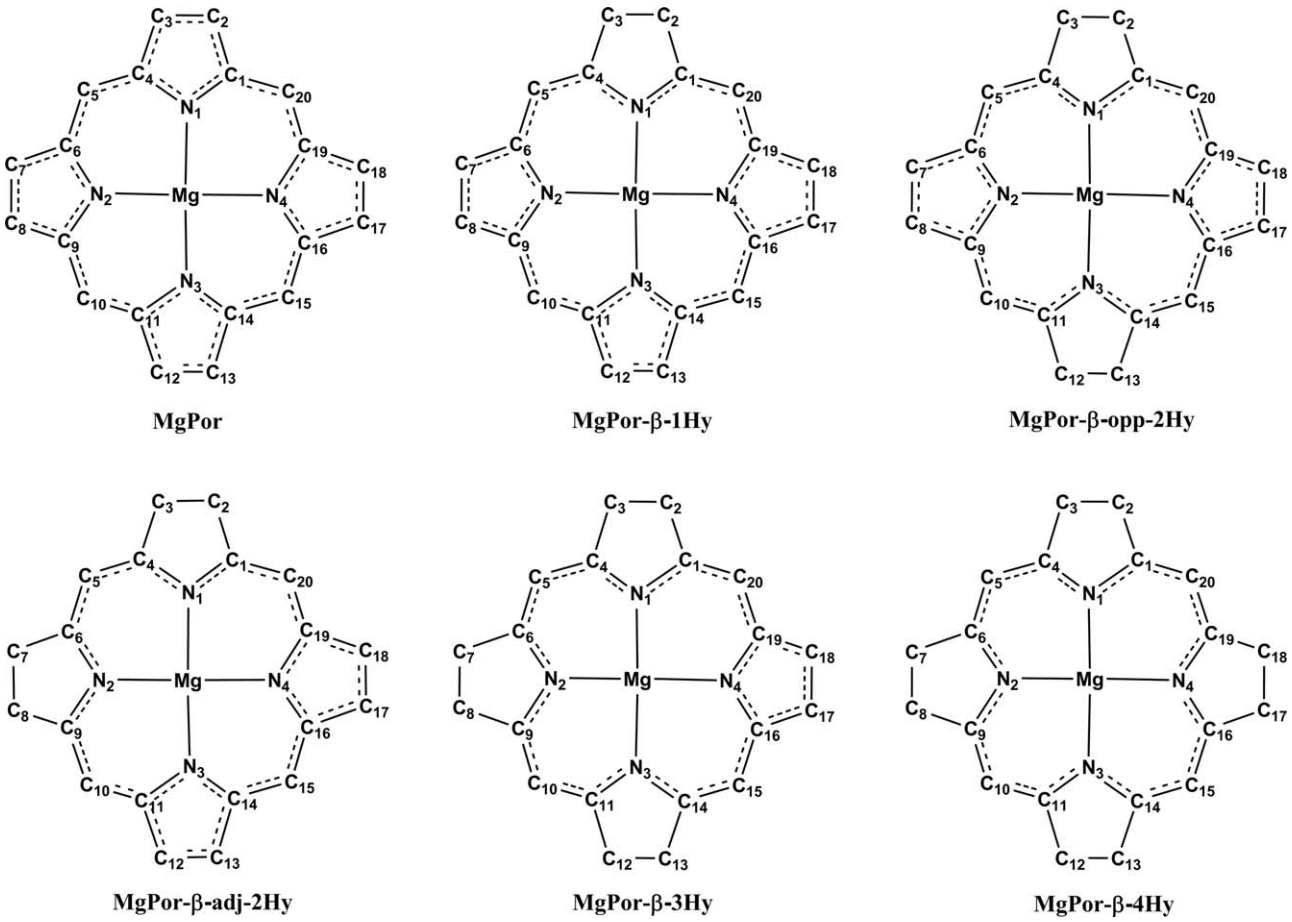

Fig. 1. Schematic molecular structures of MgPor, MgPor-β-1Hy, MgPor-β-opp-2Hy, MgPor-β-adj-2Hy, MgPor-β-3Hy, and MgPor-β-4Hy. The atomic labels are used uniformly in this paper.

In the present paper, a series of hydrogenated magnesium porphyrin complexes with different number of β-saturated pyrrolic rings, namely MgPor-β-1Hy, MgPor-β-opp-2Hy, MgPor-β-adj-2Hy, MgPor-β-3Hy, MgPor-β-4Hy, and MgPor for comparison (Fig. 1) were studied using density functional theory (DFT) and TDDFT methods to reveal the effects of the number and position of β-saturated pyrrolic rings on the electronic structures and aromatic properties of hydrogenated magnesium porphyrin derivatives. The results should be helpful for understanding the red-shift of the "orange" peak from chlorophyll *a* to bacteriochlorophyll and aromatic characteristics of metalloporphyrins, and finally for designing and synthesizing novel hydrogenated tetrapyrrole compounds sensitive to longer wavelength of sunlight.

2. Computational details

The geometries of a serious of hydrogenated magnesium porphyrin complexes (Fig. 1) were fully optimized and characterized to be local minima by harmonic vibrational frequency analysis at the B3LYP [13,14]/6-31G* level of theory. The electronic absorption spectra were simulated with TDDFT method at the same level of theory. The reliability of this method is supported by many previous theoretical works on the porphyrin derivatives [12,15–24].

In order to further verify the reliability of our TDDFT computation results, calculation at B3LYP/6-31G(d) and BP86/6-31G(d) levels for chlorophyll *a* and chlorophyll *b* were performed, respectively (Fig. S2, supplementary data).

On the basis of the above optimized geometries, the molecular orbital energies, ^{1}H NMR, magnetic susceptibility ($\Delta\chi$), and NICSs were computed at the B3LYP/6-311+G(d,p) level of theory.

The NICS values were calculated with the GIAO (gauge invariant atomic orbitals) [25] method at points 1 Å above the magnesium atom which sits in the center of 24 atoms composing the porphyrin framework. The two parameters, NICS(1) and NICS(1)*zz*, were recommended as being a better measure of the π electron delocalization as compared with NICS(0) (i.e. at the ring center) [26]. ^{1}H NMR calculation was carried out for the hydrogen atoms for the series of hydrogenated magnesium porphyrin derivatives with reference to TMS. The magnetic susceptibility (χ) values were calculated with the continuous set of gauge transformations (CSGT) method [27]. The anisotropy of magnetic susceptibility $\Delta\chi$ is defined as the difference between the out-of-plane diagonal term of the magnetic susceptibility tensor [$\chi(zz)$] and the average of the in-plane diagonal terms $\{1/2[\chi(xx)+\chi(yy)]\}$ [28].

All calculations were carried out using the Gaussian 03 program [29] on an IBM P690 system housed at Shandong Province High Performance Computing Center.

3. Results and discussion

The molecular structures of MgPor and the whole series of five hydrogenated magnesium porphyrin derivatives designed with different number of β-saturated pyrrolic rings, namely MgPor-β-1Hy, MgPor-β-opp-2Hy, MgPor-β-adj-2Hy, MgPor-β-3Hy, and MgPor-β-4Hy, are shown in Fig. 1. The atomic labels are used uniformly in this paper.

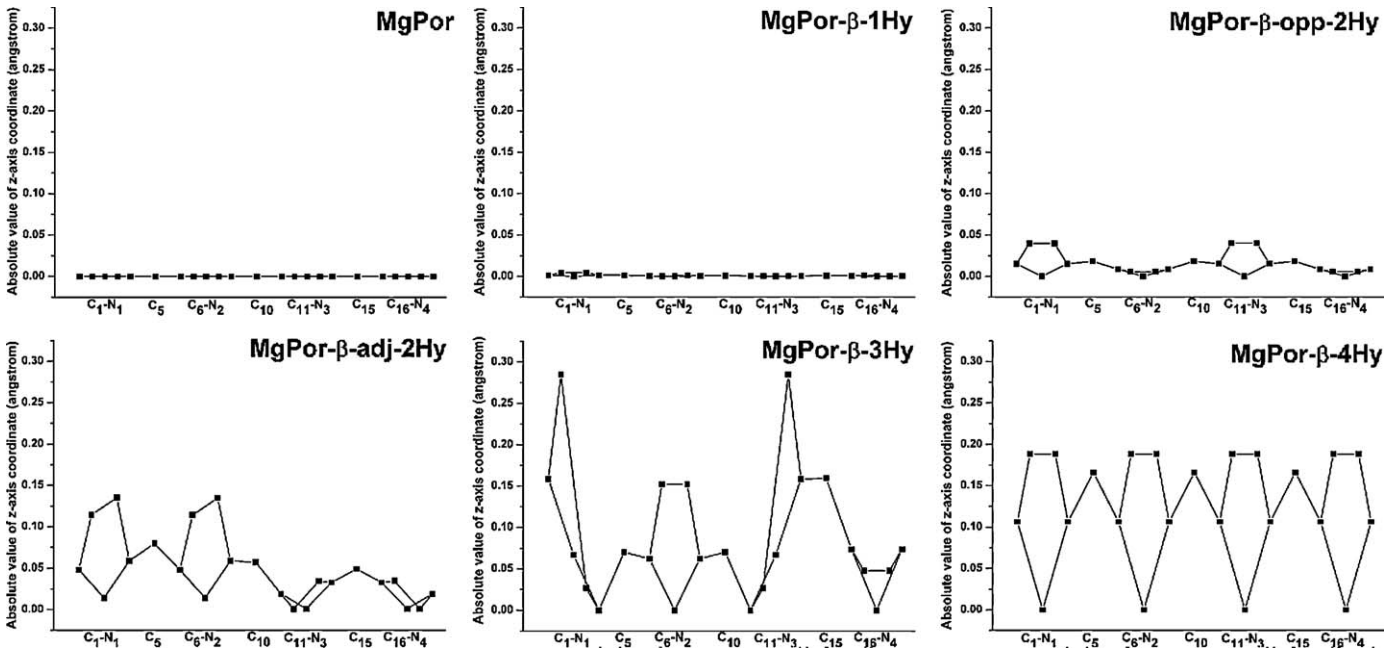

Fig. 2. The absolute value of *z*-axis coordinates of atoms (except Mg and H atoms) for MgPor, MgPor-β-1Hy, MgPor-β-opp-2Hy, MgPor-β-adj-2Hy, MgPor-β-3Hy, and MgPor-β-4Hy. *z*-Axis is perpendicular to the average molecular planes.

3.1. Molecular structures

The structures of our model molecules are mainly located in the *xy* plane. As a consequence, the flatness of the whole molecular structure could be determined by the *z*-axis coordinates of atoms except hydrogen. The planarity of molecules for MgPor and the whole series of five hydrogenated magnesium porphyrin derivatives is shown in Fig. 2 according to simulated molecular structures in terms of the absolute values of *z*-axis coordinates.

According to the calculation results, both the number and position of β-saturated pyrrolic rings dominate the change in the molecular structures of the whole series of five hydrogenated magnesium porphyrin complexes upon hydrogenation of pyrrolic rings at β-positions. As can be found, MgPor shows the D_{4h} symmetry with the *z*-axis coordinates of all atoms keeping 0 Å, indicating that the whole molecule is a completely π-conjugated system. However, the D_{4h} symmetry is destroyed when one, two, three, or four pyrrole rings are hydrogenated at the β-positions of porphyrin ring. For MgPor-β-1Hy, only the first pyrrole ring (represented by C_1–C_2–C_3–C_4–N_1, Fig. 1) is influenced by the hydrogenation with the absolute *z*-axis coordinate value of 0.001 Å for C_1 and C_4, 0.004 Å for C_2 and C_3, and 0 Å for N_1, indicating the very slight molecular structure change from MgPor to MgPor-β-1Hy. However, hydrogenation of two pyrrole rings at β-positions of porphyrin induces unnegligible change in the planarity of MgPor as indicated by the largest absolute *z*-axis coordinate values of C_3 and C_8 for MgPor-β-adj-2Hy (0.135 Å) and C_2, C_3, C_{12}, and C_{13} for MgPor-β-opp-2Hy (0.040 Å) (Fig. 2). Even the two pyrrole rings without hydrogenation were revealed to also show somewhat structural distortion despite that the twisting degree is smaller than that of the two β-saturated pyrrolic rings, which is exemplified by the absolute *z*-axis coordinate value of C_6 (0.009 Å) and C_2 (0.040 Å) for MgPor-β-opp-2Hy (Fig. 2). The results indicate that the whole structure is influenced by hydrogenation of the two pyrrole rings at β-positions. In addition, as shown in Fig. 2, the structural distortion also depends on the exact position of β-saturated pyrrolic rings. Actually, a relatively smaller degree of change in the molecular structure was revealed for MgPor-β-opp-2Hy in comparison with MgPor-β-adj-2Hy, suggesting a better π-conjugated system for the former compound. When three pyrrole rings of MgPor are hydrogenated, the structural distortion degree gets further increased as indicated by the largest absolute *z*-axis coordinate value of C_2 and C_{13} (0.285 Å) for MgPor-β-3Hy with three pyrrole rings hydrogenated at C_2, C_3, C_7, C_8, C_{12}, and C_{13} positions (Fig. 2), indicating the significant effect of the number of β-saturated pyrrolic rings on their structures. However, the compound MgPor-β-4Hy with four hydrogenated pyrrole rings does not generate the largest structural distortion with the absolute *z*-axis coordinate value of 0.188 Å for C_2, C_3, C_7, C_8, C_{12}, C_{13}, C_{17}, and C_{18}, which is smaller than that for MgPor-β-3Hy as mentioned above (Fig. 2). In fact, MgPor-β-4Hy has a saddle-shaped structure, therefore showing the D_{2d} symmetry according to our structure optimization result, which is characterized by the periodic change in absolute *z*-axis coordinate values of atoms. As shown in Fig. 2, MgPor-β-opp-2Hy also has somewhat periodic nature of structural change in absolute *z*-axis coordinate values due to its intrinsic D_2 symmetry according to the calculation results. It seems that the relative smaller structural distortion revealed for MgPor-β-opp-2Hy and MgPor-β-4Hy, in comparison with MgPor-β-adj-2Hy and MgPor-β-3Hy, respectively, is attributed to the higher symmetry of their molecular structures.

The data shown in Fig. 2 give us, in a direct manner, the information of the changing trend in the molecular structure as represented by the absolute *z*-axis coordinate values along with changing the number and position of β-saturated pyrrolic rings, which in addition is very helpful in understanding the aromatic properties of MgPor and the whole series of five hydrogenated magnesium porphyrin derivatives as discussed in the following aromatic properties section.

3.2. Molecular orbitals

Fig. 3 summarizes the energy levels of frontier molecular orbitals (FMOs) and energy gaps between the highest occupied molecular orbitals HOMO) and the lowest unoccupied molecular orbitals (LUMO) of MgPor and the series of five hydrogenated magnesium porphyrin derivatives and Table 1 summarizes the corresponding energy data. Along with the increase in the number of hydrogenated pyrrole rings, the HOMO energy of the hydrogenated

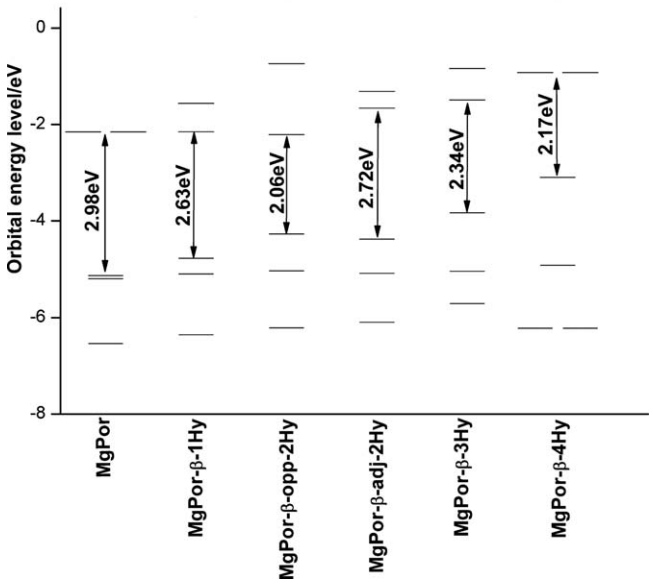

Fig. 3. The orbital energies from HOMO−2 to LUMO+1 of MgPor, MgPor-β-1Hy, MgPor-β-opp-2Hy, MgPor-β-adj-2Hy, MgPor-β-3Hy, and MgPor-β-4Hy.

porphyrinato magnesium compounds increases along with the increase in the number of hydrogenated pyrrole rings in the order of MgPor (−5.14 eV), MgPor-β-1Hy (−4.78 eV), MgPor-β-adj-2Hy (−4.38 eV), MgPor-β-opp-2Hy (−4.27 eV), MgPor-β-3Hy (−3.83 eV), and MgPor-β-4Hy (−3.10 eV). However, as clearly shown in Fig. 3, the LUMO level increases from −2.15 eV for MgPor to −0.92 eV for MgPor-β-4Hy in an irregular manner along with the increase in the number of β-saturated pyrrolic rings, resulting in the HOMO–LUMO gap increasing in the order of MgPor-β-opp-2Hy (2.06 eV), MgPor-β-4Hy (2.17 eV), MgPor-β-3Hy (2.34 eV), MgPor-β-1Hy (2.63 eV), MgPor-β-adj-2Hy (2.72 eV), and MgPor (2.98 eV). This is in good accordance with the red-shift order of the lowest energy absorption band in their electronic absorption spectra along with the increase in the number of β-saturated pyrrolic rings as detailed in the electronic absorption spectra section.

Scrutinizing the FMO distributions (Fig. 4) revealed that though the nature of FMOs is not changed upon hydrogenation at β-positions of porphyrin, the order of FMOs is altered.

The order of HOMO−1 and HOMO levels has been reversed from MgPor to the hydrogenated magnesium porphyrin derivatives (Fig. 4). The HOMO−1 of MgPor with much contribution from the pyrrole rings has been significantly affected by hydrogenation at β-positions, which generates more nodes, resulting in the much energy increment for this orbital. While the HOMO of MgPor with little contribution from the methylene-H does not change a lot. As a total result, the HOMO−1 of MgPor sensitive to the hydrogenation becomes the HOMO of hydrogenated magnesium porphyrin derivatives, while the HOMO of MgPor maintaining most of the primary distribution on the porphyrin ring changes to the HOMO−1 of hydrogenated magnesium porphyrin derivatives (Fig. 4).

Nevertheless, the fact that the HOMO energy level of the hydrogenated magnesium porphyrin compounds increases along with the increase in the number of β-saturated pyrrolic rings, as discussed above, can be well explained by the increased number of nodes generated by hydrogenation at β-positions of porphyrin in this orbital. In order to discuss the energy levels in detail, orbital contribution of methylene-H for the series of hydrogenated magnesium porphyrin compounds was calculated and the results are tabulated in Table 2. The orbital contribution of methylene-H to the HOMO for MgPor-β-opp-2Hy and MgPor-β-adj-2Hy is 6.18% and 4.61%, respectively. This is in good accordance with the higher HOMO energy level for MgPor-β-opp-2Hy than that for MgPor-β-adj-2Hy (Table 1 and Fig. 3).

After the hydrogenation at β-positions of porphyrin ring, the degenerate LUMO and LUMO+1 orbitals for MgPor become not degenerate for the hydrogenated magnesium porphyrin compounds except MgPor-β-4Hy (Table 1 and Fig. 3). As exemplified by MgPor-β-1Hy, the orbital with more contribution from the methylene-H (1.79%) becomes the LUMO+1 of MgPor-β-1Hy, while the other one with less contribution from the methylene-H (0.21%) changes to the LUMO of MgPor-β-1Hy (Table 2 and Fig. 4). This is also true for the LUMO and LUMO+1 of MgPor-β-opp-2Hy: methylene-H contributes little to the LUMO (0.26%) but has a large proportion of orbital distribution for the LUMO+1 (3.21%) (Table 2 and Fig. 4), resulting in the largest LUMO – (LUMO+1) energy gap among all the model molecules (Table 1 and Fig. 3). It is worth noting that the LUMO and LUMO+1 orbitals are not degenerate for MgPor-β-adj-2Hy, however, this compound has the smallest LUMO – (LUMO+1) energy gap in the series of hydrogenated magnesium porphyrin derivatives except MgPor-β-4Hy (Table 1 and Fig. 3), despite that these two orbitals are of very much similar distribution (Fig. 4). It is because the molecular structure of MgPor-β-adj-2Hy has no C_2 symmetry axis that the two pyrrole rings at opposite positions are not equivalent for orbital distribution. For MgPor-β-4Hy, the LUMO and LUMO+1 orbitals are degenerate due to its intrinsic D_{2d} symmetry.

It is interesting that MgPor, MgPor-β-1Hy, and MgPor-β-opp-2Hy are very similar in their the LUMO energy level (Fig. 3), since the orbital distribution of LUMO does not change very much significantly from MgPor to MgPor-β-1Hy and further to MgPor-β-opp-2Hy (Fig. 4), which is verified by the very small orbital contribution of methylene-H for the LUMO of MgPor(0), MgPor-β-1Hy (0.21%), and MgPor-β-opp-2Hy (0.26%) (Table 2). In addition, the LUMO energy increases in the order of MgPor-β-adj-2Hy, MgPor-β-3Hy, and MgPor-β-4Hy could be clarified by their LUMO orbital distribution with contribution from methylene-H with 0.75% for MgPor-β-adj-2Hy, 1.71% for MgPor-β-3Hy, and 2.66% for MgPor-β-4Hy.

As a total consequence, the number of hydrogenated pyrrole rings dominates the HOMO energy level of the series of hydrogenated magnesium porphyrin derivatives. However, both the number and position of β-saturated pyrrolic rings have great effects on the LUMO and LUMO+1 energy levels. As for HOMO−1, it is

Table 1
Calculated energy data (in eV) of the frontier molecular orbitals of MgPor, MgPor-β-1Hy, MgPor-β-opp-2Hy, MgPor-β-adj-2Hy, MgPor-β-3Hy, and MgPor-β-4Hy.

Molecules	LUMO+1	LUMO	HOMO	HOMO−1	HOMO−2
MgPor	−2.154	−2.154	−5.137	−5.203	−6.537
MgPor-β-1Hy	−1.562	−2.151	−4.778	−5.100	−6.354
MgPor-β-opp-2Hy	−0.738	−2.210	−4.274	−5.036	−6.211
MgPor-β-adj-2Hy	−1.314	−1.660	−4.380	−5.089	−6.095
MgPor-β-3Hy	−0.837	−1.490	−3.833	−5.046	−5.708
MgPor-β-4Hy	−0.923	−0.923	−3.097	−4.923	−6.217

Table 2
Molecular orbital contribution of methylene-H (in %) to HOMO, LUMO, and LUMO+1 for MgPor, MgPor-β-1Hy, MgPor-β-opp-2Hy, MgPor-β-adj-2Hy, MgPor-β-3Hy, and MgPor-β-4Hy.

Molecules	LUMO+1	LUMO	HOMO
MgPor	0.00	0.00	0.00
MgPor-β-1Hy	1.79	0.21	3.14
MgPor-β-opp-2Hy	3.21	0.26	6.18
MgPor-β-adj-2Hy	1.77	0.75	4.61
MgPor-β-3Hy	1.98	1.71	6.69
MgPor-β-4Hy	2.66	2.66	11.20

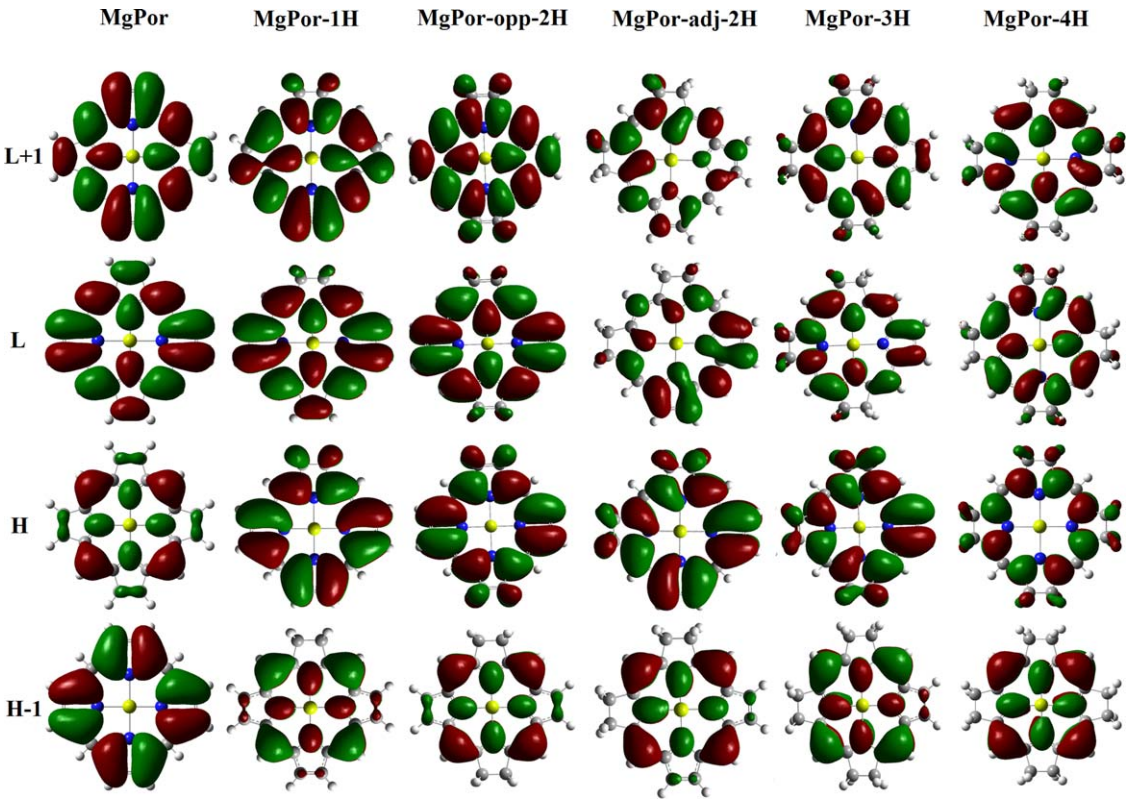

Fig. 4. Molecular orbital maps from HOMO−1 to LUMO+1 of MgPor, MgPor-β-1Hy, MgPor-β-opp-2Hy, MgPor-β-adj-2Hy, MgPor-β-3Hy, and MgPor-β-4Hy (H−1 = HOMO−1, H = HOMO, L = LUMO, L+1 = LUMO+1).

affected little by hydrogenation at β-positions of porphyrin for the whole series of hydrogenated magnesium porphyrin derivatives.

3.3. Electronic absorption spectra

Fig. 5 clearly reveals the effect of the number and position of β-saturated pyrrolic rings on the electronic absorption spectroscopic properties of the series of five hydrogenated magnesium porphyrin derivatives. The spectra of five model molecules are very similar except for some shift in absorption bands associated with different number and position of β-saturated pyrrolic rings. To ease the analysis, the whole spectrum is divided into two regions: the lowest energy absorption band as Region I and the remaining absorption bands in Region II. Compound MgPor-β-opp-2Hy exhibits the largest wavelength of the Region I band (602 nm), followed by MgPor-β-4Hy (598 nm), MgPor-β-3Hy (566 nm), MgPor-β-1Hy (530 nm), and MgPor-β-adj-2Hy (507 nm) (Table 3 and Fig. 5), revealing the significant effect of the exact positions of β-saturated pyrrolic rings on the electronic absorption spectroscopic properties of hydrogenated magnesium porphyrin derivatives.

In order to clarify the electronic transition nature for absorptions of the hydrogenated magnesium porphyrin derivatives, the spectra of the whole series of compounds were analyzed in detail in terms of band wavelength (λ/nm), oscillator strength (*f*), and orbital configurations according to theoretical calculation (Table 3).

The Region I of MgPor-β-1Hy consists of one band peaking at 530 nm (Fig. 5) due to electronic transitions from HOMO to LUMO (79%) and HOMO−1 to LUMO+1 (21%) (Table 3). Note that this band could not be considered as the traditional Q band of MgPor derivatives because the HOMO of MgPor-β-1Hy is actually the energy-raised HOMO−1 of MgPor in terms of the orbital distribution of HOMO and HOMO−1 of corresponding compounds as detailed above. Region II mainly covers the area from 300 to 400 nm with the bands involving the transitions from orbitals below HOMO−1 to LUMO/LUMO+1. Interestingly, the transition from HOMO−1 to LUMO is strongly coupled with the transition from HOMO to LUMO+1, consequently, two absorption bands at 500 and 350 nm are generated by the coupling. However, the oscillator strength of the former absorption is too weak (0.0035) for isolating an independent band in the simulated spectrum. In fact, this kind of transition coupling is more obvious in the spectra of MgPor-β-opp-2Hy (497 nm and 327 nm), MgPor-β-adj-2Hy (476 nm and 358 nm), and MgPor-β-3Hy (493 nm and 360 nm) (Table 3). Due to the degenerate LUMO and LUMO+1 orbitals and large HOMO–(HOMO−1) gap for MgPor-β-4Hy, there is no transition coupling for this compound. In addition, some electronic transitions are forbidden with the oscillator strength of the corresponding absorption bands exactly or approximately equal to 0, resulting in a very simple absorption spectrum for MgPor-β-4Hy.

Briefly summarizing above, the red-shift of the lowest energy absorption band from chlorophyll *a* to bacteriochlorophyll is reproduced by comparison of the Region I band between MgPor-β-1Hy (530 nm) and MgPor-β-opp-2Hy (602 nm). However, one may get confused that compounds MgPor-β-3Hy and MgPor-β-4Hy, which also have red-shifted Region I band according to the calculation result, are not chosen by nature. In order to clarify this question, magnetic properties such as NICS, ^{1}H NMR, and magnetic susceptibility criteria were calculated in terms of optimized molecular structures for MgPor and its hydrogenated derivatives, as detailed below.

3.4. Magnetic properties

Magnetic criteria have been studied and expected to reflect the delocalization of the π electrons and therefore the diatropicity of an aromatic system for a long time [30–32]. Among which the NICS

Table 3
Calculated wavelength (λ/nm), oscillator strength (*f*), and electron transition nature in the electronic absorption spectra of MgPor-β-1Hy, MgPor-β-opp-2Hy, MgPor-β-adj-2Hy, MgPor-β-3Hy, and MgPor-β-4Hy (only the transitions with contributions >10% are considered).

Molecules	λ/nm	*f*	Electronic transition nature [H = HOMO, L = LUMO]		
MgPor-β-1Hy	530.5	0.1148	H−0 → L+0(79%)	H−1 → L+1(21%)	
	500.4	0.0035	H−1 → L+0(60%)	H−0 → L+1(39%)	
	353.0	0.5061	H−1 → L+1(63%)	H−3 → L+0(17%)	H−0 → L+0(17%)
	350.4	0.7133	H−0 → L+1(51%)	H−1 → L+0(29%)	H−4 → L+0(11%)
	341.9	0.1296	H−3 → L+0(81%)	H−1 → L+1(13%)	
	341.3	0.1113	H−2 → L+0(86%)		
	312.9	0.2254	H−4 → L+0(87%)		
	300.7	0.0250	H−2 → L+1(96%)		
MgPor-β-opp-2Hy	602.4	0.2586	H−0 → L+0(95%)		
	497.3	0.0400	H−1 → L+0(72%)	H−0 → L+1(28%)	
	373.5	0.0000	H−2 → L+0(98%)		
	355.2	0.0191	H−3 → L+0(93%)		
	327.4	1.0083	H−0 → L+1(66%)	H−1 → L+0(30%)	
	307.2	0.0000	H−4 → L+0(87%)		
MgPor-β-adj-2Hy	507.3	0.1313	H−0 → L+0(80%)	H−1 → L+1(19%)	
	475.8	0.0337	H−0 → L+1(70%)	H−1 → L+0(29%)	
	358.0	0.5734	H−1 → L+0(67%)	H−0 → L+1(28%)	
	335.9	0.4422	H−1 → L+1(50%)	H−2 → L+0(34%)	H−0 → L+0(13%)
	326.5	0.2773	H−2 → L+0(65%)	H−1 → L+1(28%)	
	309.0	0.0595	H−3 → L+0(90%)		
MgPor-β-3Hy	565.6	0.2012	H−0 → L+0(94%)		
	492.6	0.0434	H−0 → L+1(75%)	H−1 → L+0(24%)	
	360.3	0.3475	H−1 → L+0(59%)	H−0 → L+1(19%)	H−2 → L+0(14%)
	343.3	0.0973	H−2 → L+0(86%)		
	326.6	0.0011	H−0 → L+2(98%)		
	321.3	0.0014	H−0 → L+3(99%)		
	311.0	0.4688	H−1 → L+1(87%)		
MgPor-β-4Hy	598.2	0.1916	H−0 → L+0(91%)		
	412.3	0.0000	H−0 → L+2(100%)		
	404.0	0.0000	H−0 → L+4(100%)		
	369.1	0.0020	H−0 → L+3(98%)		
	323.0	0.5887	H−1 → L+0(76%)	H−1 → L+1(11%)	

[33], ^{1}H NMR, and magnetic susceptibility criterion [34] are the most frequently used aromaticity indices.

Table 4 lists the calculated NICS(1), NICS(1)*zz*, ^{1}H NMR, χ(iso), χ(*zz*), and $\Delta\chi$ values. As can be seen, all the six parameters show aromatic characters for MgPor and its hydrogenated derivatives in similar way along with changing the number and position of β-saturated pyrrolic rings. Consequently, the calculation results are exemplified by the NICS(1)*zz* value, which is a worthy alternative magnetic criterion suggested by Schleyer and co-workers [26]. It appears that MgPor has the strongest diatropic ring current (−48.2 ppm) followed by MgPor-β-opp-2Hy (−40.5 ppm) and MgPor-β-1Hy (−39.5 ppm), then MgPor-β-4Hy (−31.4 ppm), and at last MgPor-β-adj-2Hy (−27.9 ppm) and MgPor-β-3Hy (−25.6 ppm) (Table 4), indicating the large degree of aromaticity for all the model compounds. According to the calculation results, MgPor is the most aromatic compound, MgPor-β-opp-2Hy and MgPor-β-1Hy show similar aromatic behavior, and so do MgPor-β-adj-2Hy and MgPor-β-3Hy. However, the degree of aromaticity for MgPor-β-4Hy is difficult to be quantified due to different aromatic characters indicated by different magnetic criteria in comparison with MgPor-β-adj-2Hy and MgPor-β-3Hy. It is claimed that the NICS(1)*zz* value does not depend purely on the π system but also on the σ framework of the CC and CH bonds, especially for a nonplanar molecule [35]. As mentioned above, MgPor-β-4Hy is of a saddle-shaped structure. As a consequence, $\Delta\chi$ is a more reliable quantifier of magnetic aromaticity than NICS(1)*zz*, which shows a little weaker diatropic ring current for MgPor-β-4Hy (−288.8 cgs ppm) than that for MgPor-β-3Hy (−296.2 cgs ppm) and MgPor-β-adj-2Hy (−366.6 cgs ppm) (Table 4). Nevertheless, these three compounds share similar ^{1}H NMR value with 7.3 ppm for MgPor-β-adj-2Hy, 7.0 ppm for MgPor-β-3Hy, and 7.2 ppm for MgPor-β-4Hy (Table 4). In order to eliminate the influence from

Table 4
Calculated NICS(1) (ppm), NICS(1)*zz* (ppm), ^{1}H NMR (ppm), χ(iso) (cgs ppm), χ(*zz*) (cgs ppm), and $\Delta\chi$ (cgs ppm) values of MgPor, MgPor-β-1Hy, MgPor-β-1Hy′, MgPor-β-opp-2Hy, MgPor-β-opp-2Hy′, MgPor-β-adj-2Hy, MgPor-β-adj-2Hy′, MgPor-β-3Hy, MgPor-β-3Hy′, MgPor-β-4Hy, and MgPor-β-4Hy′.

Molecules	NICS(1)	NICS(1)zz	^{1}H NMR[a]	χ(iso)	χ(*zz*)	$\Delta\chi$
MgPor	−13.9	−48.2	10.7	−330.1	−787.1	−685.6
MgPor-β-1Hy	−11.0	−39.5	9.0	−290.8	−647.3	−534.7
MgPor-β-opp-2Hy	−11.3	−40.5	9.0	−286.1	−611.8	−488.4
MgPor-β-adj-2Hy	−7.1	−27.9	7.3	−246.1	−490.5	−366.6
MgPor-β-3Hy	−6.4	−25.6	7.0	−233.6	−431.0	−296.2
MgPor-β-4Hy	−8.4	−31.4	7.2	−239.9	−432.5	−288.8
MgPor-β-1Hy′	−10.5	−38.4	9.0	−280.3	−622.3	−513.0
MgPor-β-opp-2Hy′	−10.0	−36.9	8.6	−263.1	−554.6	−437.4
MgPor-β-adj-2Hy′	−7.0	−28.0	7.4	−236.4	−474.3	−356.9
MgPor-β-3Hy′	−6.3	−25.9	7.0	−219.7	−409.0	−283.8
MgPor-β-4Hy′	−5.7	−24.0	6.5	−201.0	−338.7	−206.5

[a] Only the NMR data for ^{1}H connected to C_5 atom are presented in this table. For all the ^{1}H NMR data, readers could refer to Table S1 (supplementary data).

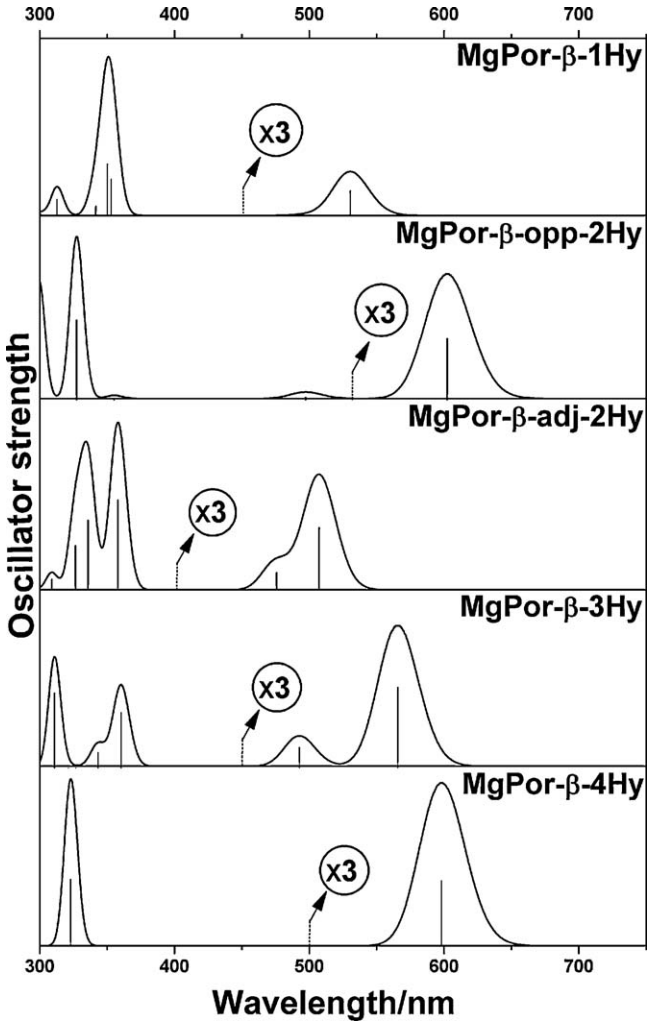

Fig. 5. Simulated electronic absorption spectra of MgPor-β-1Hy, MgPor-β-opp-2Hy, MgPor-β-adj-2Hy, MgPor-β-3Hy, and MgPor-β-4Hy.

molecular distortion on the calculated values of magnetic criteria, new structures of MgPor-β-1Hy′, MgPor-β-opp-2Hy′, MgPor-β-adj-2Hy′, MgPor-β-3Hy′, and MgPor-β-4Hy′ were designed by directly hydrogenating the corresponding β-positions of the optimized structure of MgPor with C_s symmetry and the magnetic aromaticity in terms of NICS(1), NICS(1)*zz*, ^{1}H NMR, χ(iso), χ(*zz*), and $\Delta\chi$ values for these new designed molecules was also organized in Table 4. As can be found, the aromatic behavior of MgPor-β-1Hy′ and MgPor-β-opp-2Hy′ is similar to that of MgPor-β-1Hy and MgPor-β-opp-2Hy, indicating that MgPor-β-1Hy and MgPor-β-opp-2Hy do share the same aromatic system. Again, MgPor-β-adj-2Hy′, MgPor-β-3Hy′, and MgPor-β-4Hy′ are of the similar degree of aromaticity, which is exemplified by the largest difference of NICS(1)*zz* value of 4 ppm between −28.0 ppm for MgPor-β-adj-2Hy′ and −24.0 ppm for MgPor-β-4Hy′ (Table 4). This is in good accordance with the calculation result of $\Delta\chi$ for MgPor-β-adj-2Hy, MgPor-β-3Hy, and MgPor-β-4Hy as discussed above.

In general, the six model molecules can be divided into three groups based on their degree of aromaticity. MgPor with the strongest diatropic ring current is the first group, followed by MgPor-β-1Hy and MgPor-β-opp-2Hy constituting the second group, while MgPor-β-adj-2Hy, MgPor-β-3Hy, and MgPor-β-4Hy with the weakest aromaticity belonging to the third group. However, it is worth noting that this order of aromaticity degree of model molecules could not be understood using the degree of structural distortion or previously reported proposals and aromatic pathway models for porphyrinoid aromaticity.

In order to explain the calculation results, the following hypotheses about how the π electrons of MgPor and its derivatives form the aromatic system are raised: (1) not all the π electrons are necessary for the aromatic pathway, which is verified by aromaticity research for metal free porphyrins [36]. (2) Nitrogen atoms, especially those with lone pair electrons in the *z*-axis direction, are not very favorite in a π-conjugated system since the bigger electronegativity of nitrogen than carbon atom might induce an increase in the degree of bond alternation and at the same time lead to block in the diatropic ring current. The aromatic pathways for MgPor and the series of magnesium porphyrin derivatives are shown in Fig. 6. As can be seen, two equivalent traditional 18π-[18]annulene pathways in two vertical directions, respectively, could be revealed for MgPor, which could delocalize all the π

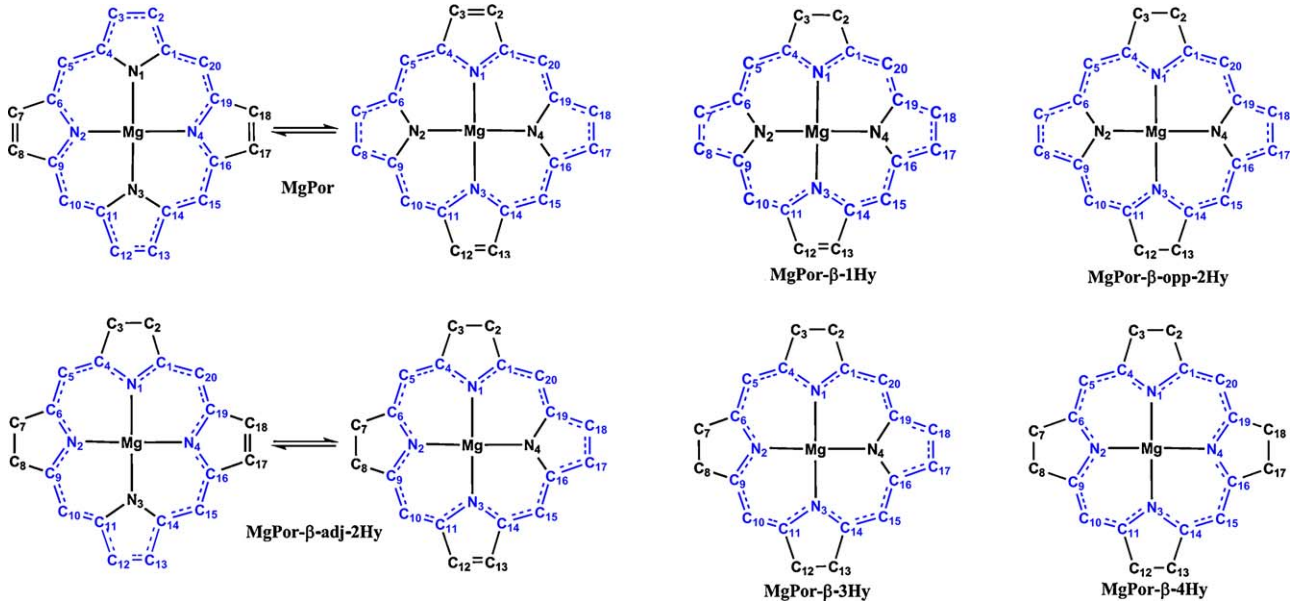

Fig. 6. The aromatic pathways for MgPor, MgPor-β-1Hy, MgPor-β-opp-2Hy, MgPor-β-adj-2Hy, MgPor-β-3Hy, and MgPor-β-4Hy.

electrons dynamically, making MgPor the most aromatic and stable compound among all the model molecules. Both of MgPor-β-1Hy and MgPor-β-opp-2Hy maintain one 18π-[18]annulene pathway, resulting in their similar values of magnetic criteria. However, the traditional 18π-[18]annulene pathway is blocked by the two β-saturated pyrrolic rings at adjacent positions in the molecular structures of MgPor-β-adj-2Hy and MgPor-β-3Hy. As a result, one nitrogen atom else with lone pair electrons in the *z*-axis direction must be included in the pathway to complete 18π electrons ring, inducing the 18π-[17]annulene pathway shown in Fig. 6. Due to the negative effect of the nitrogen atom on the diatropic ring current as discussed above, the aromaticity of MgPor-β-adj-2Hy and MgPor-β-3Hy is lower than that of molecules in the second group. Additionally, two nearly equivalent 18π-[17]annulene pathways revealed for MgPor-β-adj-2Hy (Fig. 6), could delocalize all the π electrons dynamically. This leads to a more aromatic behavior for MgPor-β-adj-2Hy in comparison with MgPor-β-3Hy. It is also noteworthy that despite the 18π-[18]annulene pathway with only two nitrogen atoms in the aromatic system, MgPor-β-adj-2Hy is thermodynamically unstable (Fig. S3, supplementary data). For MgPor-β-4Hy, the 18π-[16]annulene inner-cross is the only possible aromatic pathway (Fig. 6). According to the above-mentioned hypotheses, this aromatic pathway with four nitrogen atoms corresponds to the least aromatic character. However, MgPor-β-4Hy shows the D_{2d} symmetry and has the smallest ring size for its π-conjugated system, both of which could significantly influence the values of the magnetic criteria [30]. As a result, MgPor-β-4Hy shows similar aromaticity with MgPor-β-adj-2Hy and MgPor-β-3Hy in terms of the calculated magnetic criteria. At the end of this section, it is worth pointing out that the hypotheses raised in the present work might be not universal or even incorrect due to our limited knowledge. Further experimental and theoretical results are therefore highly desired to verify its validity and rationality.

4. Conclusion

To clarify the fact that hydrogenation of two opposite pyrrole rings could red-shift the lowest energy absorption band of chlorophyll *a*, the molecular structures, molecular orbitals, electronic absorption spectra, and magnetic properties of MgPor and a series of five well designed hydrogenated magnesium porphyrin complexes have been studied with DFT and TDDFT methods. The effects of the number and position of β-saturated pyrrolic rings on their molecular and electronic structures and aromaticity have also been clarified.

(1) Both the number and position of β-saturated pyrrolic rings dominate the change in the molecular structures of the whole series of five hydrogenated magnesium porphyrin complexes upon hydrogenation at β-positions of porphyrin rings.
(2) The number of β-saturated pyrrolic rings dominates the HOMO energy level of the series of hydrogenated magnesium porphyrin complexes. However, both the number and position of β-saturated pyrrolic rings have great effects on the LUMO and LUMO+1 energy levels. As for HOMO−1, it is affected little by hydrogenation at β-positions of porphyrin rings for the whole series of hydrogenated magnesium porphyrin derivatives.
(3) The red-shift of the lowest energy absorption band from chlorophyll *a* to bacteriochlorophyll is reproduced by comparison of the Region I bands between MgPor-β-1Hy and MgPor-β-opp-2Hy associated with the similar orbital distribution of LUMO for the two molecules and the higher HOMO energy level of MgPor-β-opp-2Hy in comparison with MgPor-β-1Hy.
(4) Natural hydroporphyrins represented by MgPor, MgPor-β-1Hy, and MgPor-β-opp-2Hy have turned out to be aromatic and stable enough. In contrast, MgPor-β-adj-2Hy, MgPor-β-3Hy, and MgPor-β-4Hy with relatively weak aromaticity seem to be unstable and therefore were not found in nature.

Acknowledgement

Financial support from the Natural Science Foundation of China, Beijing Municipal Commission of Education, China Postdoctoral Science Foundation (20090460210 and 201003051), and University of Science and Technology Beijing is gratefully acknowledged. We are also grateful to the Shandong Province High Performance Computing Center for a grant of computer time.

Appendix A. Supplementary data

Supplementary data associated with this article can be found, in the online version, at doi:10.1016/j.jmgm.2011.05.003.

References

[1] A.R. Battersby, C.J.R. Fookes, G.W.J. Matcham, E. McDonald, Biosynthesis of the pigments of life: formation of the macrocycle, Nature (London) 285 (1980) 17–21.
[2] D. Dolphin (Ed.), The Porphyrins, vols. 1–7, Academic, New York, 1978.
[3] K. Smith (Ed.), Porphyrins and Metalloporphyrins, Elsevier, Amsterdam, 1975.
[4] J.R. Bolton, Solar electricity: lessons gained from photosynthesis, in: M.H. Chisholm (Ed.), Inorganic Chemistry: Toward the 21st Century, vol. 211, American Chemistry Society, Washington, D.C., 1983, pp. 3–19.
[5] S. Fukuzumi, T. Kojima, Photofunctional nanomaterials composed of multiporphyrins and carbon-based π-electron acceptors, J. Mater. Chem. 18 (2008) 1427.
[6] J. Xiong, W.M. Fischer, K. Inoue, M. Nakahara, C.E. Bauer, Molecular evidence for the early evolution of photosynthesis, Science 289 (2000) 1724.
[7] F.P. Zscheile, C.L. Comar, Influence of preparative procedure on the purity of chlorophyll components as shown by absorption spectra, Bot. Gaz. 102 (1941) 463–481.
[8] F. Pruckner, Lichtabsorption und konstitution der chlorophyll derivate, II, Z. Physik. Chem. A 187 (1940) 257–275.
[9] J. Jusélius, D. Sundholm, The aromatic character of magnesium porphyrins, J. Org. Chem. 65 (2000) 5233–5237.
[10] A.B.J. Parusel, S. Grimme, DFT/MRCI calculations on the excited states of porphyrin, hydroporphyrins, tetrazaporphyrins and metalloporphyrins, J. Porphyrins Phthalocyanines 5 (2001) 225–232.
[11] J. Linnanto, J. Korppi-Tommola, Semiempirical PM5 molecular orbital study on chlorophylls and bacteriochlorophylls: comparison of semiempirical ab initio, and density functional results, J. Comput. Chem. 25 (2004) 123–137.
[12] L. Petit, A. Quartarolo, C. Adamo, N. Russo, Spectroscopic properties of porphyrin-like photosensitizers: insights from theory, J. Phys. Chem. B 110 (2006) 2398–2404.
[13] Y. Zhang, P. Yao, X. Cai, H. Xu, X. Zhang, J. Jiang, Density functional theory study of the inner hydrogen atom transfer in metal-free porphyrins: meso-substitutional effects, J. Mol. Graph. Modell. 26 (2007) 319–326.
[14] Q. Dong, Y. Zhang, X. Cai, J. Jiang, M. Bai, Inner hydrogen atom transfer in benzo-fused low symmetrical metal-free tetraazaporphyrin and phthalocyanine analogues: density functional theory studies, J. Mol. Graph. Modell. 27 (2009) 693–700.
[15] R. Ma, P. Guo, H. Cui, X. Zhang, M. Nazeeruddin, M. Grätzel, Substituent effect on the meso-substituted porphyrins: theoretical screening of sensitizer candidates for dye-sensitized solar cells, J. Phys. Chem. A 113 (2009) 10119–10124.
[16] R. Ma, P. Guo, L. Yang, L. Guo, X. Zhang, M. Nazeeruddin, M. Grätzel, Theoretical screening of –NH2–, –OH–, –CH3–, –F–, and –SH-substituted porphyrins as sensitizer candidates for dye-sensitized solar cells, J. Phys. Chem. A 114 (2010) 1973–1979.
[17] Y. Matano, T. Nakabuchi, T. Miyajima, H. Imahori, H. Nakano, Synthesis of a phosphorus-containing hybrid porphyrin, Org. Lett. 8 (2006) 5713–5716.
[18] M. Toganoh, H. Furuta, Theoretical study on rotation of pyrrole rings in porphyrin and N-confused porphyrin, J. Phys. Chem. A 113 (2009) 13953–13963.
[19] A.D. Becke, Density-functional thermochemistry III. The role of exact exchange, J. Chem. Phys. 98 (1993) 5648–5652.
[20] C. Lee, W. Yang, R.G. Parr, Development of the Colle-Salvetti correlation-energy formula into a functional of the electron density, Phys. Rev. B 37 (1988) 785.
[21] P. Kim, J.M. Lim, M. Yoon, J. Aimi, T. Aida, A. Tsuda, D. Kim, Excitation energy migration processes in self-assembled porphyrin boxes constructed by conjugated porphyrin dimers, J. Phys. Chem. B 114 (2010) 9157–9164.
[22] J. Šebek, P. Bouř, Ab initio modeling of the electronic circular dichroism induced in porphyrin chromophores, J. Phys. Chem. A 112 (2008) 2920–2929.
[23] J.K. Park, J.P. Chen, H.R. Lee, S.W. Park, H. Shinokubo, A. Osuka, D. Kim, Doubly β-functionalized meso–meso directly linked porphyrin dimer sensitizers for photovoltaics, J. Phys. Chem. C 113 (2009) 21956–21963.

[24] T. Honda, T. Nakanishi, K. Ohkubo, T. Kojima, S. Fukuzumi, Structure and photoinduced electron transfer dynamics of a series of hydrogen-bonded supramolecular complexes composed of electron donors and a saddle-distorted diprotonated porphyrin, J. Am. Chem. Soc. 132 (2010) 10155–10163.
[25] F. London, Théorie quantique des courants interatomiques dans les combinaisons aromatiques, J. Phys. Radium 8 (1937) 397.
[26] H. Fallah-Bagher-Shaidaei, C.S. Wannere, C. Corminboeuf, R. Puchta, P.v.R. Schleyer, Which NICS aromaticity index for planar π rings is best? Org. Lett. 8 (2006) 863–866.
[27] T.A. Keith, R.F.W. Bader, Calculation of magnetic response properties using a continuous set of gauge transformations, Chem. Phys. Lett. 210 (1993) 223.
[28] R. Carion, V. Liégeois, B. Champagne, D. Bonifazi, S. Pelloni, P. Lazzeretti, On the aromatic character of 1,2-dihydro-1,2-azaborine according to magnetic criteria, J. Phys. Chem. Lett. 1 (2010) 1563.
[29] M.J. Frisch, G.W. Trucks, H.B. Schlegel, G.E. Scuseria, M.A. Robb, J.R. Cheeseman, J.A. Montgomery Jr., T. Vreven, K.N. Kudin, J.C. Burant, J.M. Millam, S.S. Iyengar, J. Tomasi, V. Barone, B. Mennucci, M. Cossi, G. Scalmani, N. Rega, G.A. Petersson, H. Nakatsuji, M. Hada, M. Ehara, K. Toyota, R. Fukuda, J. Hasegawa, M. Ishida, T. Nakajima, Y. Honda, O. Kitao, H. Nakai, M. Klene, X. Li, J.E. Knox, H.P. Hratchian, J.B. Cross, C. Adamo, J. Jaramillo, R. Gomperts, R.E. Stratmann, O. Yazyev, A.J. Austin, R. Cammi, C. Pomelli, J.W. Ochterski, P.Y. Ayala, K. Morokuma, G.A. Voth, P. Salvador, J.J. Dannenberg, V.G. Zakrzewski, S. Dapprich, A.D. Daniels, M.C. Strain, O. Farkas, D.K. Malick, A.D. Rabuck, K. Raghavachari, J.B. Foresman, J.V. Ortiz, Q. Cui, A.G. Baboul, S. Clifford, J. Cioslowski, B.B. Stefanov, G. Liu, A. Liashenko, P. Piskorz, I. Komaromi, R.L. Martin, D.J. Fox, T. Keith, M.A. Al-Laham, C.Y. Peng, A. Nanayakkara, M. Challacombe, P.M.W. Gill, B. Johnson, W. Chen, M.W. Wong, C. Gonzalez, J.A. Pople, Gaussian 03, Revision B. 05, Gaussian, Inc., Pittsburgh, PA, 2003.
[30] Z. Chen, C.S. Wannere, C. Corminboeuf, R. Puchta, P.v.R. Schleyer, Nucleus-independent chemical shifts (NICS) as an aromaticity criterion, Chem. Rev. 105 (2005) 3842–3888.
[31] T. Heine, C. Corminboeuf, G. Seifert, The magnetic shielding function of molecules and pi-electron delocalization, Chem. Rev. 105 (2005) 3889–3910.
[32] P.v.R. Schleyer, H. Jiao, What is aromaticity? Pure Appl. Chem. 68 (1996) 209.
[33] P.v.R. Schleyer, C. Maerker, A. Dransfeld, H. Jiao, N.J.Rv.E. Hommes, Nucleus-independent chemical shifts: a simple and efficient aromaticity probe, J. Am. Chem. Soc. 118 (1996) 6317.
[34] H.J. Dauben Jr., J.D. Wilson, J.L. Laity, Diamagnetic susceptibility exaltation as a criterion of aromaticity, J. Am. Chem. Soc. 90 (1968) 811.
[35] U. Fleischer, W. Kutzelnigg, P. Lazzeretti, V. Mûhlenkamp, IGLO study of benzene and some of its isomers and related molecules. Search for evidence of the ring current model, J. Am. Chem. Soc. 116 (1994) 5298.
[36] T.D. Lash, S.A. Jones, G.M. Ferrence, Synthesis and characterization of tetraphenyl-21,23-dideazaporphyrin: the best evidence yet that porphyrins really are the [18]annulenes of nature, J. Am. Chem. Soc. 132 (2010) 12786–12787.